THE JOURNAL OF PHYSICAL CHEMISTRY A

Article

pubs.acs.org/JPCA

# Heterogeneous Uptake and Adsorption of Gas-Phase Formic Acid on Oxide and Clay Particle Surfaces: The Roles of Surface Hydroxyl Groups and Adsorbed Water in Formic Acid Adsorption and the Impact of Formic Acid Adsorption on Water Uptake

Gayan Rubasinghege,[†] Saralyn Ogden,[†] Jonas Baltrusaitis,[‡] and Vicki H. Grassian*[,†]

[†]Department of Chemistry, University of Iowa, Iowa City, Iowa 52242, United States

[‡]Faculty of Science & Technology, University of Twente, Enschede, The Netherlands

Supporting Information

**ABSTRACT:** Organic acids in the atmosphere are ubiquitous and are often correlated with mineral dust aerosol. Heterogeneous chemistry and the uptake of organic acids on mineral dust particles can potentially alter the properties of the particle. In this study, heterogeneous uptake and reaction of formic acid, HCOOH, the most abundant carboxylic acid present in the atmosphere, on oxide and clays of the most abundant elements, Si and Al, present in the Earth's crust are investigated under dry and humid conditions. In particular, quantitative adsorption measurements using a Quartz Crystal Microbalance (QCM) coupled with spectroscopic studies using Attenuated Total Reflection Fourier Transform Infrared (ATR-FTIR) spectroscopy are combined to allow for both quantification of the amount of uptake and identification of distinct adsorbed species formed on silica, alumina, and kaolinite particle surfaces at 298 K. These oxides and clay particles show significant differences in the extent and speciation of adsorbed HCOOH due to inherent differences in surface −OH group reactivity. Adsorbed water, controlled by relative humidity, can increase the irreversible uptake of formic acid. Interestingly, the resulting layer of adsorbed formate on the particle surface decreases the particle hydrophilicity thereby decreasing the amount of water taken up by the surface as measured by QCM. Atmospheric implications of this study are discussed.

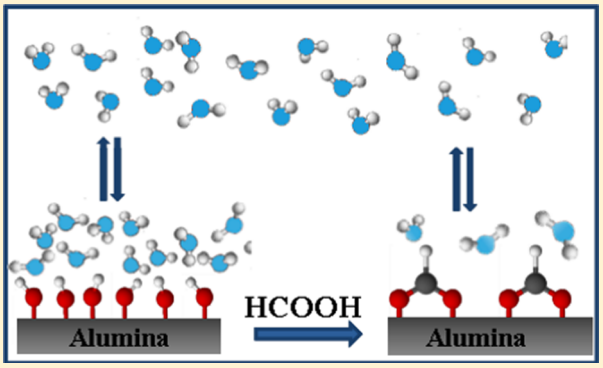


## INTRODUCTION

Heterogeneous chemistry of atmospheric trace gases on mineral dust particles has been an area of great interest in the past decade, due to its significance in altering the chemical balance of the atmosphere and modifying the properties of these particles.[1−3] Mineral dust particles in the atmosphere can undergo chemistry in both gas and liquid phases due to reactions at the gas−solid and liquid−solid interfaces.[4,5]

Past studies on heterogeneous chemistry of mineral dust aerosol have focused mainly on inorganic trace gases, including nitrogen oxides,[6−8] ozone,[9,10] and sulfur dioxide.[11,12] Organic compounds are ubiquitous in the atmosphere and are thought to play an important role in the acidity of the atmosphere as well as involved in heterogeneous chemistry on aerosol surfaces.[13] In numerous field studies, organic acids in particular have been correlated with mineral dust. A recent article summarizing the progress in understanding physical and chemical properties of African and Asian mineral dust particles has suggested that attention be given to the interaction of organic acids on dust.[14] Lee and co-workers,[15] during the Atlanta Super Site Project, reported that approximately 40% of the analyzed particles (0.35−2.5 $\mu$m size range) contained fragments associated with organic acids. Russell et al. has showed organic acids can increase both the rate of dissolution and solubility of minerals similar to the inorganic acids.[16] Heterogeneous uptake of organic acids on mineral particles can affect mechanisms and thus the kinetics of weathering and diagenesis.[17]

While other organic acids such as propionic, citric, tartaric, malonic, and butyric occur as minor constituents, formic acid is the most prevalent carboxylic acid in the gas phase with reported concentrations from 0.05−6 ppbv gas-phase[18,19] and can be as high as 20 ppb.[20,21] In some regions, the mixing ratio of formic acid can exceed that of $HNO_3$ and HCl.[19] This makes formic acid an important molecule in understanding its role in atmospheric chemistry. Because of its low molecular weight, high polarity, and quite high solubility, atmospheric formic acid is responsible for a significant portion of the acidity in rainwater; up to 64% in more remote regions[22] and up to 35% in North America.[23] While formic acid thus influences pH dependent chemical reactions in clouds, it further increases the

**Received:** August 15, 2013
**Revised:** September 27, 2013
**Published:** September 30, 2013



   dx.doi.org/10.1021/jp408169w | J. Phys. Chem. A 2013, 117, 11316−11327

oxidative capacity of the troposphere via interaction with NOx and HOx cycles that regulate tropospheric $O_3$ level.[24,25]

Even though sources of atmospheric formic acid have been well recognized and include various anthropogenic (automobiles, biomass, and coal combustions) and biogenic (oxidation of olefins and isoprenes) emissions,[21] its sinks are still poorly understood, even on regional scales.[26] Major loss pathways for formic acid in the troposphere include wet and dry deposition, which accounts for 95% of HCOOH,[27] and slow gas-phase reaction with OH radicals.[18] The large uncertainties in these removal mechanisms of HCOOH, including its interaction with mineral dust, have led to difficulties in determining its tropospheric lifetime in atmospheric models. Estimates of the residence times of HCOOH vary from weeks to hours.[28,29] Therefore, it has become vital to understand the rates, mechanisms, and products of the surface reaction between formic acid and mineral dust particles in order to understand its role in the troposphere.

Previous studies on organic acid adsorption on mineral aerosol components such as $SiO_2$, $Fe_2O_3$, $CaCO_3$, and $Al_2O_3$ at 295 K report that uptake is sufficiently large that dust may be a significant sink for organic acids in the atmosphere.[1,21,30,31] In fact, calculated lifetimes of formic acid are much shorter than that for slow removal of HCOOH by OH radical. However, there remain uncertainties in the analysis of species formed on the surface and different reaction mechanisms under ambient conditions. Given increasing evidence of the importance of water in atmospheric chemistry,[32] it can be asked, how does adsorbed water impact the reactivity of mineral dust in terms of enhancing or inhibiting reaction rates and how does adsorbed water impact the stability of species once formic acid is adsorbed on the surface. According to Al-Hosney et al.[30] and Tong et al.,[31] the uptake of formic acid can be expected to be enhanced at higher RH conditions typical of the ambient troposphere. Reaction chemistry occurring in these adsorbed water layer may differ from bulk aqueous phase chemistry.[33] Furthermore, following uptake of formic acid, the hydroscopic behavior of mineral dust particles can be significantly altered by species adsorbed on the particle surface. This can impact the behavior of these particles in the atmosphere including their water content, size, optical properties, and CCN activity.[34] Given the fact that mineral dust aerosol represents different minerals of different phase and composition, these impacts will depend on the chemical composition and phase of the mineral under investigation.

The current study focuses on heterogeneous uptake and reaction of gas-phase formic acid with various model oxides and clay components of dust, the role of water in these reactions, and the effect that these reactions have on the water uptake behavior of these component dust particles. The findings of this study is key to better understanding the underlying fundamental chemistry involved and, from this, a better understanding of these reactions in the atmosphere. In particular, heterogeneous reactions of formic acid on different model components of mineral dust of some of the most earth abundant minerals, including oxides (silica and alumina) and clays (kaolinite), under different water-activity regimes (dry and humid), have been investigated. Vibrational spectroscopy is used to determine surface speciation of adsorbed products, however, quantitative analysis of surface coverage can be difficult to obtain. Therefore, a flow system that allows for simultaneous measurements from Attenuated Total Reflection Fourier Transform Infrared (ATR-FTIR) spectroscopy and Quartz Crystal Microbalance (QCM) is used as these techniques provide spectroscopic information about the coordination to the surface and quantitative mass measurements, respectively. Furthermore, quantum chemical calculations are performed in order to better understand the formation of irreversibly adsorbed species and the different coordination modes to the surface.

## EXPERIMENTAL SECTION

**Materials.** The oxide and clay particles used in this study are composed of the most abundant elements present in the Earth's crust: oxygen, silicon, and aluminum. All chemicals were reagent grade or better and were used as received. Commercially available silica ($SiO_2$, Degussa), alumina ($\gamma$-$Al_2O_3$, Degussa), and kaolinite (Source Clay (KGa-1b)) were used. Formic acid uptake experiments were carried out with the vapor of a concentrated formic acid source (Alfa Aesar). Sample preparation for FTIR and QCM applications, water uptake experiments, and solution preparation were done using aqueous suspensions in optima water (Fisher Scientific).

**Sample Preparation for ATR-FTIR Spectroscopy and QCM Measurements.** For ATR-FTIR experiments, a sample of known mass (ca. 15 mg) was suspended in 1 mL of optimum water. After sonication for 10 min, the suspension was spread evenly onto an AMTIR crystal. Complete drying was allowed overnight, in the presence of a dry air ($CO_2$ and $H_2O$ free) flow before the sample was analyzed. XPS and FTIR analysis confirmed there were minimal contaminates prior to formic acid exposure. For QCM measurements, a similar suspension was made to deposit onto the quartz resonator. In this case, the sample was sprayed from a custom designed atomizer onto a QCM crystal.[35−37] A dry air flow is passed through the colloidal suspension and pushed through a small opening whereby particles are deposited from the aerosol mist onto the QCM crystal. The spray of particles on to the crystal is done for a length of time such that enough sample is completely covered with a thin layer of particles. Complete drying of the sample under a steady stream of dry air was done overnight in a final step before formic acid uptake experiments began.

It should be noted that good contact is needed between the dried sample and the crystal, in both ATR and QCM experiments. This typically occurred but did not always occur resulting in poor signal (ATR) or unstable measurements (QCM). For QCM measurements, it was also determined that a sample mass between 30−50 $\mu$g across the crystal was best for depositing a thin, uniform sample layer on the crystal and for ensuring not too much sample was on the QCM, otherwise mass changes were not linearly proportional to the frequency.

**Uptake Measurements Using a Combined ATR-FTIR Spectroscopy and QCM Approach.** Formic acid adsorption studies were conducted in a custom built flow system and described in detail elsewhere.[35,36] A Thermo Nicolette 6700 FTIR spectrophotometer and a QCM200, 5 MHz quartz crystal microbalance from Stanford Research Systems were integrated into the flow system for additional sample analysis. A commercial attenuated total reflection (ATR) horizontal liquid cell apparatus (Pike Technology) was placed in the internal compartment of the spectrometer. The bottom portion of the liquid cell, supplied by Pike Technology, was used as is. The top portion of the liquid cell was redesigned to contain inlet and outlet ports for humidified air, reactive gases, and a Honeywell HIH-3602-L relative humidity sensor for in situ measurements of relative humidity.


dx.doi.org/10.1021/jp408169w | J. Phys. Chem. A 2013, 117, 11316−11327

Dry air coming into the system was allowed to flow through a set of water bubblers at a controlled rate producing humidified air. This was then mixed and equilibrated with dry air inside the mixing chamber before being directed toward the oxide films prepared for QCM and ATR-FTIR measurements. The relative humidity was controlled by varying the flow of dry air through the system of water bubblers, while allowing the system to equilibrate for 30 min at each flow. The uptake of water at each humidity level was observed using FTIR and QCM measurements, while the relative humidity was recorded using the humidity sensor and a custom-built digital readout.

HCOOH uptake was conducted in a similar way to the water uptake measurements but at a single steady flow of 100 sccm of dry air over the top of the formic acid solution. Even though the oxides and clays used in this study show an uptake of HCOOH at lower HCOOH pressures, higher flow rates were used to distinguish the unique spectral features in the ATR-FTIR spectra under experimental conditions of higher relative humidities. A calibration was done to convert the units of flow into appropriate pressure units. While monitoring the uptake using FTIR and QCM measurements, reversible and irreversible were quantified using the QCM and the corresponding ATR-FTIR spectrum to quantify and characterize both irreversibly and reversibly bound HCOOH.

**Quantum Chemical Methods.** Periodic ab initio solid state program suite CRYSTAL09 was used in all calculations.[38,39] The program used functions localized at atoms as the basis for expansion of the crystalline orbitals via linear combination of atomic orbitals (LCAO) technique. All-electron Gaussian type basis sets were used. Basis sets have been obtained from the University of Torino CRYSTAL basis set library (accessed Spring 2012). Namely, 85-11d1G basis set was used for Al[40] and 6-31d1G for O and C.[41] The hybrid B3LYP[42,43] Hamiltonian was used in all calculations. The DFT exchange−correlation contribution is evaluated by numerical integration over the unit cell volume. Radial and angular points of the grid were generated through Gauss−Legendre radial quadrature and Lebedev two-dimensional angular point distributions with a pruned grid of 75 radial and 974 angular points. The level of accuracy in evaluating the Coulomb and Hartree−Fock exchange series was controlled by five parameters,[38] and values of 7, 7, 7, 7, and 14 were used. The reciprocal space integration was performed by sampling the Brillouin zone with the 4 × 4 × 1 Pack−Monkhorst net.[44] Structure optimizations were performed using analytical energy gradients with respect to atomic coordinates and unit-cell parameters,[45−47] within a quasi-Newton scheme combined with the Broyden−Fletcher−Goldfarb−Shanno scheme for Hessian updating.[48−51] Convergence was checked on both gradient components and nuclear displacements and was signaled when root-mean-square (rms) gradient was 0.00003 hartree/Bohr and rms displacement was 0.00012 Bohr. A SCF convergence criterion on total energy was set to $10^{-11}$ Hartree. Both cell parameters and atomic positions were optimized in bulk structure optimization, whereas cell parameters were fixed in surface slab optimization. All calculations were performed using spin restricted formalism.

Initial aluminum oxide crystalline cell parameters as well as the atomic coordinates were taken from Digne et al.[52] and fully optimized. Using these optimized parameters, a (100) surface supercell was built and used in adsorption studies. Optimization of supercells was performed in fixed cell parameters, only atomic positions were allowed to relax. No atomic position constraints were applied. Vibrational frequencies were calculated using numerical evaluation of the first-derivative of the analytical atomic gradients. No negative frequencies were calculated confirming minima on the PES surface.

For comparison, cluster-type calculations were performed utilizing a rigid $\gamma$-$Al_2O_3$ surface fragment carved out of the perfect crystal. Unsaturated valencies of the cluster were saturated with hydrogen atoms in the direction of the Al−O bond with a fixed 0.97 Å distance. The position of the cluster atoms were fixed during the geometry optimization, and only the adsorbate molecule was allowed to relax. Consequentially, frozen modes were projected out of the Hessian and vibrational frequencies of formic acid only were calculated. Cluster-type calculations were performed using Gaussian09 revision B01.[53] A combination of M05-2X functional[54] and 6-311++G(d,p) basis set was used.

## RESULTS AND DISCUSSION

**Characterization of Particles and Particle Surfaces.** The three proxies for mineral dust, silica, alumina, and kaolinite, used in this study possess interesting chemical characteristics with unique surface and bulk properties. Microscopy images for representative samples are provided in Supporting Information Figure S1. These images show that these samples are different from each other in shape and size. As discussed in Hudson et al.[55] the irregular shaped clay particles have shape factor, $\chi$, ranging from 1.2 to 1.3, where $\chi$ = 1 is a sphere. The shape factors for silica and alumina samples used were ∼1 suggesting that particles were more spherically shaped. The average particle sizes, determined based on TEM and SEM images were 20 (±3) nm, 13 (±2) nm, and >2 $\mu$m with corresponding BET surface areas of 230 (±5), 101 (±4), and 10.7 (±0.5) $m^2/g$, for silica, alumina, and kaolinite, respectively. These surface areas are used to calculate coverages of adsorbed formic acid and water on these different samples as discussed in further detail below.

ATR-FTIR spectroscopy can also provide insights into the surface chemical and physical properties of the particles under investigation. ATR-FTIR spectra of each of the source minerals after overnight drying at less than 5% RH are shown in Figure 1. Characterization with ATR-FTIR spectroscopy showed more

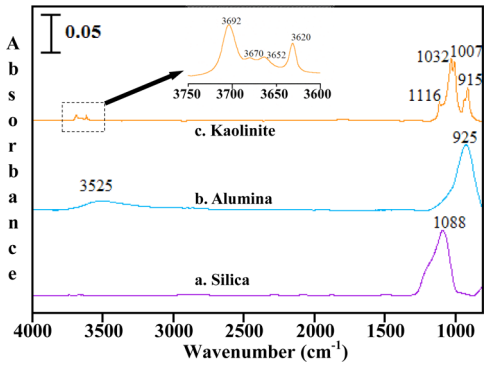


**Figure 1.** ATR-FTIR spectra of (a) silica, (b) alumina, and (c) kaolinite under dry (<1% RH) conditions. The inset is the enlarged spectral region from 3600 to 3750 $cm^{-1}$ for kaolinite, which was assigned to the characteristic bands associated with the OH-stretch of the inner-surface hydroxyl groups. The spectral region from 800 to 1600 $cm^{-1}$ contains the fundamental characteristic absorptions for each of the minerals.


dx.doi.org/10.1021/jp408169w | J. Phys. Chem. A 2013, 117, 11316−11327

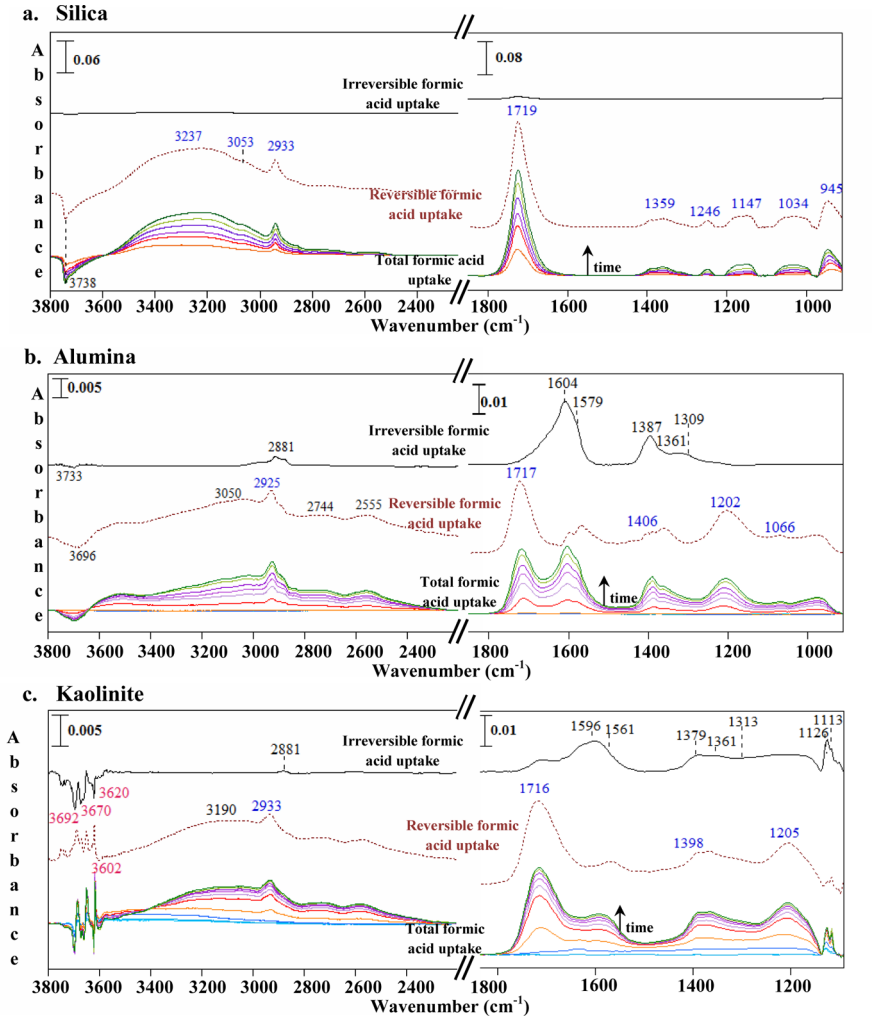


**Figure 2.** Formic acid adsorption on (a) silica, (b) alumina, and (c) kaolinite. Time-course ATR-FTIR spectra recorded following exposure to HCOOH (at 100 sccm) under dry (<1% RH) conditions at 298 K. The FTIR spectra, recorded as a function of time in the presence of HCOOH flow, are labeled "total formic acid uptake". Exposure of formic acid reacted surfaces to dry air without formic acid vapor yields loss of weakly bound species leaving a strongly bound chemisorbed formic acid species adsorbed on the particle surface. These spectra are labeled as "irreversible formic acid uptake". The FTIR spectrum of "irreversible acid uptake" is subtracted from "total formic acid uptake" spectrum with the saturation uptake of HCOOH to obtain vibrational modes of molecularly bound species and labeled as "reversible formic acid uptake". The peaks can be assigned to reversible-molecular and dissociative-irreversible surface uptake of HCOOH (see Table 1 and 2).

pronounced differences in the OH stretching region (3000–3500 $cm^{-1}$) and in the lattice phonon modes (~1000 $cm^{-1}$). Distinct absorption bands at 3692, 3670, 3652, and 3620 $cm^{-1}$ in the spectrum for kaolinite arise from the OH-stretching modes of outer- and inner-surface hydroxyl groups in various octahedral and tetrahedral sites within the clay structure.[56−59] A recent study by White et al. discuss important structural properties of these inner-surface −OH groups in detail, with a specific focus on −OH structure and exchange reactions.[59] These inner-surface hydroxyl groups are structurally important for kaolinite. Strong absorptions observed near or below 1000 $cm^{-1}$ arise from lattice vibrations or phonon modes, which is more structured in kaolinite compared to silica and alumina. In silica and alumina, IR absorptions corresponding to Si−O and Al−O stretch can be observed at 1088 and 925 $cm^{-1}$, respectively. These lattice vibrations can be observed at 1116, 1032, 1007, and 915 $cm^{-1}$ for the kaolinite sample. The frequencies of the vibrational bands observed in this study are in good agreement with literature values for these different oxide and clay particles.[56,60]

**Quantitative Molecular, Reversible Surface Adsorption of Formic Acid on Silica.** The uptake of formic acid on silica particle surfaces was studied under dry conditions, i.e., in the absence of water vapor. The FTIR spectrum of gas-phase HCOOH inside the flow system under dry conditions is shown in Supporting Information Figure S2. The spectrum consists of intense vibrational bands corresponding to monomer configuration of gas-phase formic acid. These peaks include those at 3569, 2942, 1776, and 1105 $cm^{-1}$, and the assignments of these bands are given in Supporting Information Table S1.[61,62] Weaker vibrations at 3100, 1362, and 1215 $cm^{-1}$ suggest the presence of some dimers, estimated to be less than 5% of the gas phase.[61,62]

ATR-FTIR spectra following the reaction of HCOOH on silica particles at a flow of 100 sccm (100 ± 1 mTorr), at 298 K, as a function of exposure time for a period of 120 min are shown in Figure 2a. In the presence of HCOOH flow, the FTIR spectra, recorded as a function of time, in Figure 2 are labeled "total formic acid uptake". Exposure of formic acid reacted surface to dry air without formic acid vapor results in

Table 1. Vibrational Assignments of Molecularly Adsorbed Formic Acid on Silica, Alumina, and Kaolinite

| | vibrational frequencies from current study | | | reference vibrational frequencies | | |
|---|---|---|---|---|---|---|
| | | | | lit/exptl | | |
| vibrational mode | silica | $\gamma$-$Al_2O_3$ | kaolinite | silica[63] | $\alpha$-$Al_2O_3$[26,64,65] | calculated for silica[61] |
| $\upsilon$(OH) (MOH) | 3738 | 3733 | 3692 | | | |
| | | 3696 | 3670 | | | |
| | | | 3620 | | | 3631 |
| | | | 3602 | | | |
| $\upsilon$(OH) (COH) | 3053 br. | 3050 br. | 3190 br. | | 2921 | 3214 |
| $\upsilon$(CH) | 2933 | 2925 | 2933 | 2950 | 2562 | 2944 |
| $\upsilon$(C═O) | 1719 | 1717 | 1716 | 1722 | 1706 | 1714 |
| $\delta$(CH) | 1359 | 1406 | 1398 | | | 1364 |
| $\delta$(OH) | | | | | | 1322 |
| $\upsilon$(C−O) | 1246 | 1202 | 1205 | | | 1191 |
| $\gamma$(CH) | 1147 | 1066 | | | | 1039 |

the loss of these bands from the spectrum indicating the desorption of weakly bonded formic acid. This process is referred to as the reversible uptake of formic acid. The assignments of the vibrational bands of formic acid adsorbed on silica particles are given in Table 1. As it can be seen in Figure 2a, exposure of silica surface to gas-phase HCOOH results in adsorbed formic acid species on the surface with a concomitant decrease in the frequency of isolate −OH groups, as indicated by the negative intensity at 3738 $cm^{-1}$ in the −OH stretching region.[6] When the silica surface is then exposed to dry air without formic acid vapor, the bands immediately decrease in intensity and disappear from the spectrum indicating a loss of weakly or molecularly bound formic acid that can be referred to as the reversible uptake of formic acid.

The vibrational frequencies observed in this study agree well with the reported values for molecularly bonded formic acid on metal oxide surfaces as shown in Table 1.[63] In a recent theoretical study by Iuga et al.[61] on the adsorption of a single formic acid molecule on different silicate surface models using quantum-mechanical methods, it has been reported that out of all possible energy minimized adsorption geometries, the adsorption complex involving the carbonyl O atom and the hydroxyl H atom of HCOOH interacting with a silanol group and O atom of the siloxane Si−O−Si bridge, respectively, is the most stable configuration (Figure 3a). Our experimental data further confirm these findings with a good agreement to their calculated vibrational frequencies for this particular surface complex with the lowest rms values.

**Uptake of Formic Acid on Alumina and Kaolinite: Evidence for Reversible and Irreversible Adsorption of Formic Acid.** Uptake of formic acid on alumina and kaolinite particle surfaces at a flow of 100 sccm (100 ± 1 mTorr) under dry conditions (<1% RH) at 298 K are shown in Figure 2b and c, respectively. In contrast to silica surface, these FTIR spectra provide information on the vibrational modes of different surface species adsorbed to the particle surface. In particular, there is the presence of a surface species that is molecular, reversibly bonded, similar to silica, on the surface and a second species that irreversibly bonds to the surface and is dissociative in nature. This leaves the strongly bonded chemisorbed formic acid species on the particle surface.

These spectra are labeled as "irreversible formic acid uptake" in Figure 2. The FTIR spectrum of "irreversible formic acid uptake" is subtracted from "total formic acid uptake" spectrum to obtain vibrational modes of molecularly bound species and labeled as "reversible formic acid uptake" in Figure 2. The sum

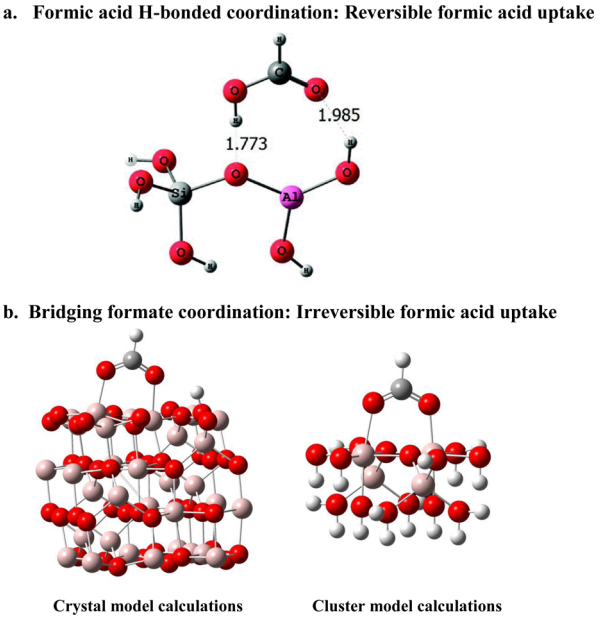


**Figure 3.** Energy minimized model structures for formic acid uptake. (a) Hydrogen-bonded formic acid uptake via H-bonding involving the carbonyl O atom and the hydroxyl H atom of HCOOH interacting with a silanol group and O atom of the siloxane Si−O−Si bridge, respectively. Adapted and reproduced with the permission from ref 61. Copyright 2012 American Chemical Society. (b) Bridged formate adsorbed on alumina optimized using periodic crystal and cluster model calculations. Atoms of different elements are highlighted with different colors: metal sites, red; oxygen, pink/purple; aluminum, gray; carbon, white; hydrogen. Calculated vibrational frequencies are given in Table 3

of reversible and irreversible formic acid uptake is the spectrum labeled total formic acid at the last time point in the time series shown.

As can be seen in the spectra shown in Figure 2b,c, exposure of both alumina and kaolinite to gas phase HCOOH results in adsorbed formic acid species on the surface (ca. 900−1800 $cm^{-1}$) with a loss of surface −OH groups, as confirmed by the negative intensities in the −OH region (ca. 3400−3800 $cm^{-1}$). On the basis of this analysis, spectral bands at 2925, 1717, 1406, 1202, and 1066 $cm^{-1}$ in Figure 2b can be clearly assigned to the molecular adsorption of HCOOH on the alumina particle surface as given in Table 1.[26,64,65] Absorption bands associated with "irreversible formic acid uptake" in Figure 2b can be


dx.doi.org/10.1021/jp408169w | J. Phys. Chem. A 2013, 117, 11316−11327

**Table 2. Vibrational Assignments of Formate Anion on Silica, Alumina, and Kaolinite**

| | experimental frequencies from current study | | reference vibrational frequencies for $\alpha$-$Al_2O_3$ | | | |
|---|---|---|---|---|---|---|
| | | | | lit/calcd[31] | | |
| vibrational mode | $\gamma$-$Al_2O_3$ | kaolinite | exptl[26,31,66−68] | monodentate | bidentate | bridged |
| $\upsilon$(CH) | 2881 | 2881 | 2867 | | | |
| $\upsilon_{as}$(OCO) | 1604 | 1596 | 1590 | 1651 | 1513 | 1606 |
| $\upsilon_{s}$(OCO) | 1387 | 1379 | 1393 | 1268 | 1362 | 1393 |
| $\delta_{bend}$(CH) | 1361 | 1361 | 1378 | 1367 | 1260 | 1383 |

assigned to the dissociative-irreversible adsorption of formic acid on alumina and are given in Table 2. Since there are no other data present in the literature for the assignment of vibrational modes of formate adsorbed on the gamma phase of alumina, vibrational assignments for formate adsorbed on the alpha phase of alumina were used as a reference. The bands at 2881 and 1361 $cm^{-1}$ associated with C−H stretching and bending modes, respectively, are in line with the assignment on other alumina surfaces.[66−68] The absence of C═O and C−OH stretch modes in the IR spectrum for "irreversible uptake" suggests that the reaction of the HCOOH on the surface to give the chemisorbed formate anion.[69] Here, we observe OCO symmetric and asymmetric stretch modes at 1387 and 1604 $cm^{-1}$, respectively; those are characteristic to the adsorbed formate ion.[26,31] In comparing the FTIR spectra of alumina with that of kaolinite, shown in Figure 2c, there are no significant differences in the vibrational modes and both are in good agreement with the literature. Yet, differences can be observed in the loss of surface −OH groups on these two surfaces which will be discussed in detail in the following section. In addition, on the basis of the difference in relative intensities of the peaks assigned to reversible and irreversible uptake, it can be suggested that the kaolinite surface shows a greater amount of reversible uptake compared to that of the alumina surface. Quantitative analysis of formic acid uptake is provided from QCM measurements, as discussed in the next section.

There can be three possible modes of coordination of the formate ion: monodentate, whereby one carboxylate oxygen is coordinated to a surface Al atom; bidentate, whereby two carboxylate oxygens are bonded to the same Al atom; bridging, whereby two oxygens of carboxylate are coordinated to two different surface Al atoms.[31] Vibrational frequencies of the $\upsilon_{(OCO)}$ band provide information about the mode of coordination of adsorbed species on the surface.[70,71] Quantum chemical calculation can provide molecular insight of the vibrational frequencies as well as structural parameters to better understand the different modes of coordination of adsorbed HCOOH on metal oxide surfaces. Results from the current study agree with the bridged conformation of adsorbed HCOOH, proposed in the previous theoretical studies for $\alpha$-$Al_2O_3$ (Table 2).[31] Here, we extend the analysis of IR frequencies of dissociative-irreversible HCOOH to the gamma phase of adsorbed alumina by utilizing both periodic and cluster type vibrational frequency calculations. Vibrational frequencies corresponding to formate adsorbed on gamma alumina surface with a bridged conformation are given in Table 3. The dissociated bridged configuration of adsorbed formate for crystalline and cluster models are shown in Figure 3b. Typically, both periodic and cluster type methods are used interchangeably to model vibrational frequencies of the adsorbed molecules. Cluster type calculations are subject to

**Table 3. DFT Calculation Using Periodic Crystal and Cluster Models for Formate Anion Adsorbed on $\gamma$-$Al_2O_3$ with Bridged Coordination**

| | | calculated frequencies in the current study | |
|---|---|---|---|
| vibrational mode | experimental frequencies from the current study | crystal model | cluster model (scaled)[a] |
| $\upsilon$(CH) | 2881 | 3062 | 3092 (2968) |
| $\upsilon_{as}$(OCO) | 1604 | 1621 | 1674 (1607) |
| $\upsilon_{s}$(OCO) | 1387 | 1419 | 1450 (1392) |
| $\delta_{bend}$(CH) | 1361 | 1385 | 1397 (1341) |

[a]Vibration frequencies when a typical scaling factor of 0.96[74,75] is applied to the bridged cluster model.

finite size effects. Binuclear cluster models, for example, used before for HCOOH adsorption modeling on $\alpha$-$Al_2O_3$,[31] typically do not exactly represent the exact interatomic Al−Al distance found in the crystal but nevertheless provide useful information about distortion of the moiety bonded to the cluster and accurate vibrational frequencies.[72] Furthermore, clusters can represent defect sites on the particle surface for stepped or vacancy type cases.

Fundamental vibrational modes of HCOOH above 1000 $cm^{-1}$ are $\upsilon$(OH), $\upsilon$(CH), $\nu$(C═O), $\upsilon_{bend}$(CH), $\delta_{bend}$(OH), and $\upsilon$(C−O).[73] The same vibrations are present for molecularly adsorbed HCOOH. When HCOOH dissociatively adsorbs, the $\upsilon$(OH) vibration is absent, and distinct bands due to $\upsilon$(C═O) and $\upsilon$(C−O) vibrations start resembling those of the more delocalized $OCO^-$ moiety as $\upsilon_{as}$(OCO) and $\upsilon_{s}$(OCO), respectively. Both $\upsilon$(OH) and $\upsilon$(CH) are overestimated in both the models due to the lack of anharmonicity correction. Notably, while the $\upsilon$(C═O) is slightly overestimated from the experimental data, it is shifted toward lower wavenumbers for more strongly bonded formic acid and is closest to the observed experimental value of 1604 $cm^{-1}$. If a typical scaling factor of 0.96[74,75] is applied to the bridged (O−C−O) cluster model, this frequency is then 1607 $cm^{-1}$, the same as experimental, indicating that the bridged coordination is present on the surface. A calculated value of 1621 $cm^{-1}$ for bridged chemisorbed HCOOH in crystal models also agrees with the experimental frequencies without any scaling.

It is difficult to generalize when comparing cluster and crystal calculations values given in Table 3 due to the use of different functionals, basis sets, and local bonding configurations. Since the cluster size is fixed, no metal atom relaxation can proceed in cluster model calculations. For the bridged adsorption case, however, the calculated cluster model frequencies are


dx.doi.org/10.1021/jp408169w | J. Phys. Chem. A 2013, 117, 11316−11327

consistently larger by 30, 53, 31, and 12 $cm^{-1}$ for the frequencies listed in Table 3. This rather systematic difference implies that both clusters describe frequencies relatively accurately semiquantitatively and therefore can be compared. Older comparisons of hybrid density functionals concluded that there is very similar rms error of 34 $cm^{-1}$ for both B3LYP and B3P86 with the calculates scaling factor almost the same (0.9613 vs 0.9559) for the same 6-31G* basis set.[75] Recent data in frequency scaling factors database[76] showed that, for within the functional with a different basis set, vibrational frequencies do not change that much and that essentially the same scaling factor can be used, but the scaling factor slightly varies between different functionals.

**Quantitative Analysis Using QCM.** In cases where both reversible and irreversible uptake may occur, it is difficult to quantitatively assess the amounts of irreversible and reversible uptake. However, QCM measurements can be used to quantify these different processes. The frequency change of the quartz resonator can be related to the increase in mass on the crystal as given by the Sauerbrey equation given in eq 1.

$$\Delta f = -C_f \Delta m \tag{1}$$

where $\Delta f$ is the change in frequency of the resonator, $\Delta m$ is the change in mass related to the change in frequency ($\mu g/cm^2$), and $C_f$ is the sensitivity factor, which is a constant of 56.6 Hz $cm^2/\mu g$ for a 5 MHz AT-cut quartz crystal.[36,77] A thin layer of the sample is first sprayed on QCM crystal, and the initial mass of the deposited sample is determined using the decrease of the QCM frequency. Adsorption or desorption of a substance on to or from the thin film would cause a further change in mass. According to the Sauerbrey equation, this change would be coupled to a change in frequency of resonance of the quartz crystal resonator. Mass of adsorbed formic acid ($\Delta m$) from the above measurements can be further converted into surface coverage ($S_{HCOOH}$), molecules of adsorbed formic acid per unit area of sample, by normalizing to the BET surface area of the sample, as follows:

$$S_{HCOOH}\left(\frac{g}{cm^2}\right) = \frac{\Delta m \cdot A \cdot 10^{-6}}{M \cdot SA_{BET} \cdot 10^4} \tag{2}$$

and, converting to molecules per $cm^2$, yields

$$S'_{HCOOH}\left(\frac{molecules}{cm^2}\right) = \frac{S_{HCOOH}}{MW} \cdot N \tag{3}$$

where $A$ is the surface area of the QCM crystal (0.4 $cm^2$), $M$ is the mass of the sample deposited on the QCM crystal (g), $SA_{BET}$ is the measured BET surface area of the sample ($m^2/g$), $MW$ is the molecular weight of formic acid, and $N$ is Avogadro's number. Therefore, the mass of HCOOH adsorbed or any other adsorbate for that matter can be probed by using QCM measurements. Moreover, simultaneously collecting FTIR data further allowed us to attribute specific absorption features to reversibly and irreversibly surface-bound species.

QCM measurements for HCOOH uptake on silica, alumina, and kaolinite are shown in Figure 4, and a quantitative view of total, reversible, and irreversible surface coverage of adsorbed HCOOH on the three particle surfaces analyzed are given in Table 4. It should be noted that all the data given here are normalized to the respective surface area and a drift in QCM frequency during the measurement is taken into account (see dashed line in Figure 4) in the calculations. It can be seen that contrary to the higher surface area indicated by silica particles, it

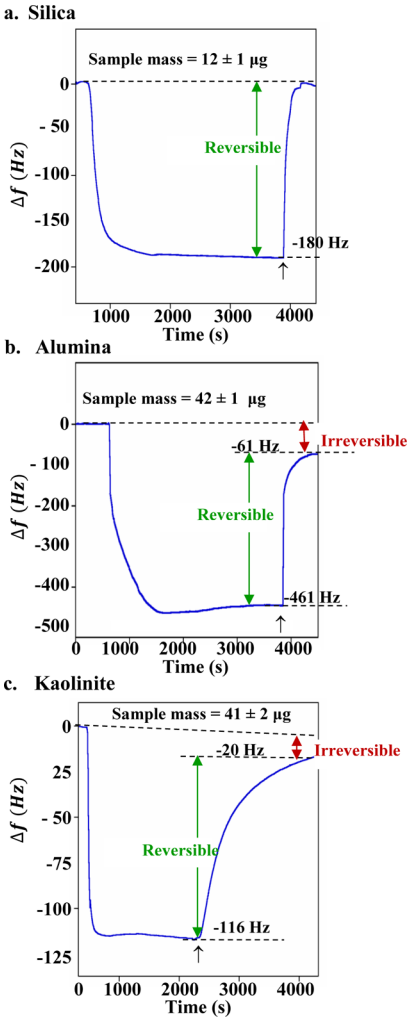


**Figure 4.** Formic acid uptake on (a) silica, (b) alumina, and (c) kaolinite at a flow of 100 sccm monitored with QCM measurements as $f$(time). The arrow (↑) indicates the time that the air flow switches from air containing $HNO_3$ vapor to just dry air.

showed the lowest saturation coverage of total HCOOH and no irreversibly bound HCOOH. The highest total and irreversible uptake HCOOH was observed on the alumina surface. Interestingly, in spite of lower surface area, kaolinite particles showed relatively higher total HCOOH uptake than silica and similar reversible uptake compared to alumina surface. Moreover, in all the three samples, reversible uptake dominates over irreversible uptake of HCOOH, yet to different extents. Therefore, these data suggest that the extent as well as the nature of adsorption of HCOOH on mineral surfaces is mineral type-dependent and that these variation are attributed the differences of their surface −OH groups in the following section.

**Role of OH Groups in the Adsorption of Formic Acid.** Heterogeneous uptake of HCOOH on silica, alumina, and kaolinite (Figure 2) results in negative peaks around 3600−3800 $cm^{-1}$ that can be attributed to the involvement of surface −OH groups in surface adsorption.[78,79] In the case of silica, a negative band at 3738 $cm^{-1}$ has been previously assigned to isolated −OH groups terminated on the silica particle surface.[6] A decrease in the intensity of this peak indicates that formic acid molecules interacting with these isolated surface −OH groups on the silica surface. Given the fact that silica surface


dx.doi.org/10.1021/jp408169w | J. Phys. Chem. A 2013, 117, 11316−11327

Table 4. Saturation Surface Coverage for Adsorbed HCOOH at 298 K

| sample | surface coverage (molecules/cm$^2$) | | |
|---|---|---|---|
| | total adsorbed HCOOH | reversibly adsorbed HCOOH | irreversibly adsorbed HCOOH |
| silica | 1.3 (±0.3) × $10^{15}$ | 1.3 (±0.3) × $10^{15}$ | |
| alumina | 2.5 (±0.7) × $10^{15}$ | 2.2 (±0.6) × $10^{15}$ | 0.3 (±0.1) × $10^{15}$ |
| kaolinite | 1.7 (±0.5) × $10^{15}$ | 1.4 (±0.5) × $10^{15}$ | 0.3 (±0.1) × $10^{15}$ |

only shows reversible uptake, it can be suggested that these surface −OH groups are hydrogen-bonded to HCOOH and that this then gives rise to the broad peak centered at 3237 cm$^{-1}$. Alumina, in contrast to silica, shows two negative peaks at 3696 and 3733 cm$^{-1}$. The peak at 3696 cm$^{-1}$ has been assigned to isolated −OH groups on the alumina surface, and they form H-bonds with the physisorbed HCOOH. This is confirmed by the fact that this peak is regenerated upon desorption of weakly bound HCOOH in the presence of dry air. The second negative band at 3733 cm$^{-1}$ can be attributed to surface −OH groups coordinated to tetrahedral Al surface sites[80] and generally identified as more basic hydroxyl groups.[79] Previous studies on adsorption acidic gases, i.e., $HNO_3$, by our group[6] and others[81] have reported that these −OH groups are consumed during the uptake of these gases and yield coadsorbed water on the surface. Thus, the chemical reaction between gas-phase HCOOH and surface −OH groups can be described as

$$HCOOH(g) + -OH^-(a) \rightarrow HCOO^-(a) + H_2O(a) \quad (4)$$

Formation of water as a byproduct is further confirmed by the two spectral bands at 1635 cm$^{-1}$ at the initial stage of adsorption and the broad band around 3500 cm$^{-1}$, which are assigned to the bending and stretching modes of the coadsorbed water. It can be seen from the FTIR spectra that −OH stretching region for kaolinite shows more structure than that of silica and alumina. The negative peaks at 3692, 3670, 3620, and 3602 cm$^{-1}$ can be attributed to OH-stretching motion of inner-surface hydroxyl groups in various positions within the clay structure.[56] These hydroxyl groups are structurally important for kaolinite because they keep the clay from swelling. Thus, these negative spectral features suggest that, in kaolinite, surface hydroxyl groups on both external surface and potentially in the inner layers actively participate in the uptake of HCOOH. The involvement of the inner-surface hydroxyl groups in the reaction can be the reason, in part, for the observed higher reversible uptake in kaolinite compared to silica surface. The differences observed for the HCOOH uptake can be thus attributed to these variations in the mode and molecular density of different surface −OH groups, which is characteristic to a particular mineral surface. Further, these data highlight the importance of distinct surface hydroxyl groups, in particular having −OH groups on both external surface and inner layers, during the heterogeneous uptake of HCOOH.

**Effect of Relative Humidity and Impact of Adsorbed HCOOH on Hygroscopic Behavior.** It has been shown that hydroscopicity of a particle surface influences not only the water content but also particle size, chemical reactivity, and optical properties of the particle.[34] Mixing state of the aerosol particle with organic and inorganic compounds can be vital in determining the hydroscopic nature of a particular reactive surface. Numerous field studies have confirmed that heterogeneous reaction on mineral dust particles always influence their hygroscopicity.[82−84] Studies in our laboratory[6,7] and others[8] have shown that surface adsorption of inorganic ions, i.e., nitrate and sulfate, on metal oxides can influence water uptake. A recent study by Ma et al.[34] reports that heterogeneous reaction of acetic acid with metal oxides (MgO and $\alpha$-$Al_2O_3$) and carbonates ($CaCO_3$) effect the hygroscopic behavior of these particles. They have further shown that the extent of this effect varies with mineral phase. In the current study, $\gamma$-$Al_2O_3$ was used as the model surface to investigate the hydroscopic behavior of mineral particles in the presence of adsorbed formic acid.

Here, we focused on the impact of adsorbed formate on the water uptake of alumina particle surfaces. FTIR spectra of alumina particles coated with a thin layer of adsorbed formate as a function of relative humidity are shown in Figure 5. With

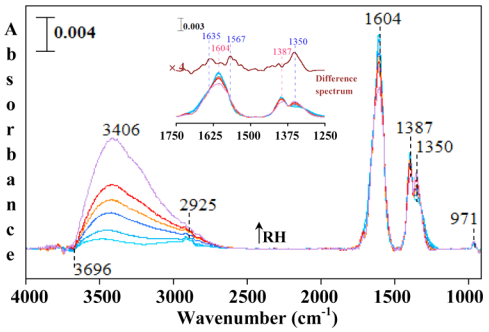


**Figure 5.** ATR-FTIR spectra of alumina surface with adsorbed formate, resulted from the reaction with formic acid, exposed to increasing relative humidity (<1 to 80% RH) at 298 K. Several changes are observed in the spectrum following exposure to water, shifts in frequency and intensity are seen for some of the absorption bands. Inset: Enlarged region from ca. 1800 to 1200 cm$^{-1}$, and the difference spectrum was obtained by subtracting the spectrum at <1% RH from the spectrum at highest RH.

the increase of RH, there is the growth of a band at approximately 3406 cm$^{-1}$, which is due to the stretching mode of adsorbed water. In addition, there are changes in the adsorbed formate ion spectrum in the $\nu_3$ region. These changes are more apparent in the Figure 5 inset that is blown up of the spectral region ca. 1800 to 1200 cm$^{-1}$. The growth of the bending mode of adsorbed water can be seen at 1635 cm$^{-1}$ in the difference spectrum. At the lower relative humidity values (<20% RH), absorptions due to bridged formate, as well as several new bands, are observed as the relative humidity is increased. At higher relative humidity, a clear loss in adsorbed bridged formate is observed, whereas new intense absorption bands begin to grow further with frequencies at ∼1567 and 1350 cm$^{-1}$. These changes suggest that these two bands can be assigned to the $\nu_3$ mode of adsorbed formate associated, i.e., H-bonded, with coadsorbed water. The similar splitting (∼217 cm$^{-1}$) in the frequencies of the $\nu_3$ band, compared to dry conditions, and red shift in OCO stretching implies a partial solvation of the molecular ion in the presence of coadsorbed water.


dx.doi.org/10.1021/jp408169w | J. Phys. Chem. A 2013, 117, 11316−11327

The difference in water uptake between the aluminum oxide samples with and without the formic acid coating was further compared by QCM measurements. The water uptake measurements collected using QCM for the unreacted alumina sample is shown in Figure 6a, whereas the alumina reacted with formic acid is shown in Figure 6b. As discussed above, changes in frequency can be used to determine the mass of water adsorbed on the substrate at each corresponding relative humidity by using the Sauerbrey equation, which can be converted into mass of water per unit mass (mg/g) or unit area ($\mu$g/cm$^2$) of sample. These data are shown in Figure 6c for both reacted and unreacted alumina. These water adsorption isotherms highlight significant difference between formic acid reacted and unreacted alumina. Previous studies have suggested that one monolayer of adsorbed water for unreacted alumina particles is ~20% RH.[6] Under similar RH conditions, surface water coverage on formic acid reacted sample is limited to ~0.1 monolayer. Even at higher relative humidity, ~80% RH, reacted alumina surface does not show monolayer coverage of adsorbed water. A higher relative humidity, corresponding to one monolayer of water adsorbed, always refers to a higher hydrophobicity, thus these results suggest that reaction with HCOOH decreases the hydrophilicity of the particles and enhances the hydrophobic properties of the alumina particles.

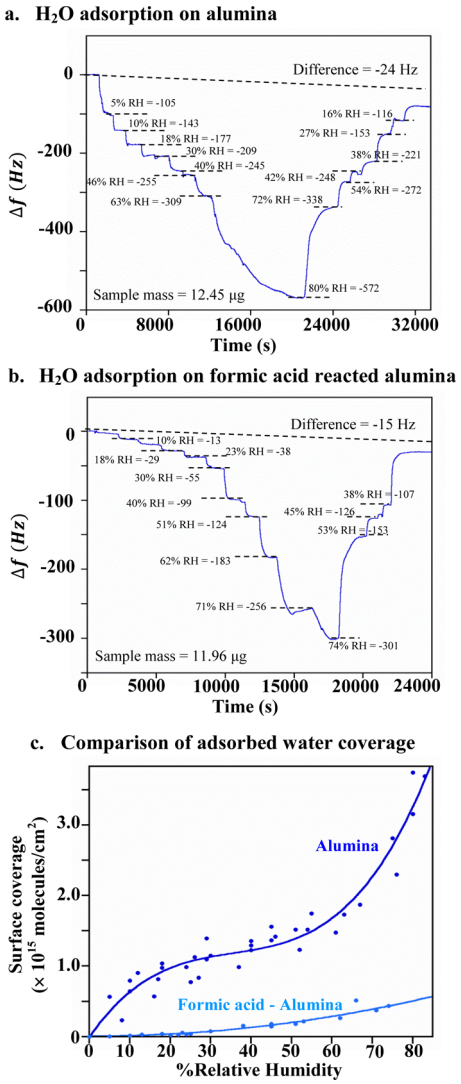


**Figure 6.** Water uptake on (a) alumina and (b) alumina reacted with formic acid, monitored with QCM measurements as $f$(RH). (c) Data in panels a and b, along with several other experiments, were converted into the surface coverage of water adsorbed on the alumina surface as a function of RH. The solid line in panel c represents the BET fit of the experimental data.

While these data show how the uptake of water on a formic acid coated aluminum oxide surface is impacted, it is also important to gain an understanding of the effect of water on formic acid uptake. Here, formic acid is introduced simultaneously with water vapor, as a function of the water vapor pressure, while collecting QCM measurements. These data are shown in Figure 7. QCM measurements for each relative humidity were recorded after exposing the above reacted samples to dry air without formic acid and water vapor. Since water is reversibly adsorbed on the surface, the change in mass on QCM only corresponds to the amount of irreversibly bonded formic acid, in the form of adsorbed formate on the alumina surface. Interestingly, these data show that humid conditions favor the irreversible bonding of formate. This can be due to the solvation of ions at interfaces that could enhance the dissociation of HCOOH to yield adsorbed formate and protons at the surface.

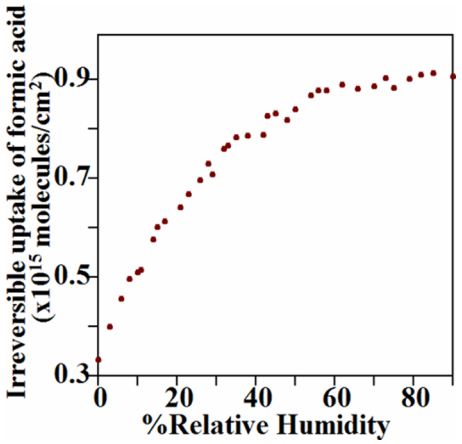


**Figure 7.** Impact of adsorbed water, controlled by relative humidity, on the uptake of HCOOH on alumina particle surfaces. Simultaneous adsorption of formic acid (100 sccm) as a function of relative humidity was monitored using QCM. These data illustrates the change of molecular density of irreversibly adsorbed formate as $f$(RH). The amount of formate was determined with QCM after the sample was purged with dry air to remove the water layer leaving behind adsorbed formate.

## CONCLUSIONS AND ATMOSPHERIC IMPLICATIONS

In this study, the effect of relative humidity and the role of hydroxyl groups on uptake of HCOOH, an important atmospheric gas, on distinct oxide and clay particle surfaces, silica, alumina, and kaolinite, were investigated. The combined approach of QCM measurements and ATR-FTIR spectroscopy allowed for quantification of the amount of uptake, identification of distinct adsorbed species, and the quantitative abundance of these. Characterization data using ATR-FTIR spectroscopy from the three different mineral oxides highlights the presence of distinct hydroxyl groups with significant differences in their respective surface densities on specific external and internal surfaces. Analysis of IR spectra showed


dx.doi.org/10.1021/jp408169w | J. Phys. Chem. A 2013, 117, 11316−11327

loss of specific hydroxyl groups, and formic acid uptake on distinct mineral oxide surfaces takes place through the association of HCOOH with these −OH groups. Formic acid molecules reversibly adsorb on silica surface forming H-bonds with the isolated surface −OH groups. On alumina, in addition to isolated −OH groups, surface −OH groups coordinated to tetrahedral Al surface sites also participate in the HCOOH uptake yielding an irreversibly bound thin layer of formate on the surface. More interestingly, involvement of surface −OH groups in the inner layers of kaolinite further enhances its reactivity toward HCOOH uptake. These differences are reflected in the quantitative analysis of total, reversible, and irreversible uptake of HCOOH using QCM measurements.

Relative humidity plays a key role in the formic acid reaction with mineral oxide surfaces. Higher relative humidity favors the total and irreversible uptake of formic acid on alumina surface. Yet, this thin coating of adsorbed formate on the particle surface significantly enhances the hydrophobic nature of the surface. Lower water content on mineral particle surface limits heterogeneous reactions, in particular with water-soluble gases (e.g., NOx and SOx). In a recent study on synergistic effects between HCOOH and $SO_2$, Wu et al.[1] further report that heterogeneous reaction of HCOOH is hindered significantly by coexisting $SO_2$, and the total amount of formate is decreased during coadsorption on the particle surface, whereas the total amount of sulfate was not affected during coadsorption on the surface. Therefore, processed aerosols in the presence of organic acids may behave differently in the atmospheric reactions that warrant further investigation.

## ■ ASSOCIATED CONTENT

### Supporting Information

(1) TEM and SEM images of silica, alumina, and kaolinite; (2) FTIR spectrum of gas-phase HCOOH; (3) vibrational modes assignment of gas-phase formic acid, HCOOH; and (4) complete ref 53. This material is available free of charge via the Internet at http://pubs.acs.org.

## ■ AUTHOR INFORMATION

### Notes

The authors declare no competing financial interest.

## ■ ACKNOWLEDGMENTS

This material is based on the work supported by the National Science Foundation under grant CHE-0952605 and CHE-1305723. Any opinions, findings, and conclusions or recommendations expressed in this material are those of authors and do not necessarily reflect the views of the National Science Foundation.

## ■ REFERENCES

(1) Wu, L. Y.; Tong, S. R.; Zhou, L.; Wang, W. G.; Ge, M. F. Synergistic Effects between $SO_2$ and HCOOH on Alpha-$Fe_2O_3$. *J. Phys. Chem. A* **2013**, *117*, 3972−3979.

(2) Rossi, M. J. Heterogeneous Reactions on Salts. *Chem. Rev.* **2003**, *103*, 4823−4882.

(3) Cwiertny, D. M.; Young, M. A.; Grassian, V. H. Chemistry and Photochemistry of Mineral Dust Aerosol. *Annu. Rev. Phys. Chem.* **2008**, *59*, 27−51.

(4) Dentener, F. J.; Carmichael, G. R.; Zhang, Y.; Lelieveld, J.; Crutzen, P. J. Role of Mineral Aerosol as a Reactive Surface in the Global Troposphere. *J. Geophys. Res.* **1996**, *101*, 22869−22889.

(5) Johnson, E. R.; Grassian, V. H. *Environmental Catalysis of the Earth's Atmosphere: Heterogeneous Reactions on Mineral Dust Aerosol in Environmental Catalysis*; Grassian, V. H., Ed.; CRC Publishing: Boca Raton, FL, USA, 2005.

(6) Goodman, A. L.; Bernard, E. T.; Grassian, V. H. Spectroscopic Study of Nitric Acid and Water Adsorption on Oxide Particles: Enhanced Nitric Acid Uptake Kinetics in the Presence of Adsorbed Water. *J. Phys. Chem. A* **2001**, *105*, 6443−6457.

(7) Goodman, A. L.; Underwood, G. M.; Grassian, V. H. Heterogeneous Reaction of $NO_2$: Characterization of Gas-Phase and Adsorbed Products from the Reaction, $2NO_2(g) + H_2O(a) \rightarrow HONO(g) + HNO_3(a)$ on Hydrated Silica Particles. *J. Phys. Chem. A* **1999**, *103*, 7217−7223.

(8) Finlayson-Pitts, B. J.; Wingen, L. M.; Sumner, A. L.; Syomin, D.; Ramazan, K. A. The Heterogeneous Hydrolysis of $NO_2$ in Laboratory Systems and in Outdoor and Indoor Atmospheres: An Integrated Mechanism. *Phys. Chem. Chem. Phys.* **2003**, *5*, 223−242.

(9) Mogili, P. K.; Kleiber, P. D.; Young, M. A.; Grassian, V. H. Heterogeneous Uptake of Ozone on Reactive Components of Mineral Dust Aerosol: An Environmental Aerosol Reaction Chamber Study. *J. Phys. Chem. A* **2006**, *110*, 13799−13807.

(10) Chen, H. H.; Stanier, C. O.; Young, M. A.; Grassian, V. H. A Kinetic Study of Ozone Decomposition on Illuminated Oxide Surfaces. *J. Phys. Chem. A* **2011**, *115*, 11979−11987.

(11) Baltrusaitis, J.; Cwiertny, D. M.; Grassian, V. H. Adsorption of Sulfur Dioxide on Hematite and Goethite Particle Surfaces. *Phys. Chem. Chem. Phys.* **2007**, *9*, 5542−5554.

(12) Nanayakkara, C. E.; Pettibone, J.; Grassian, V. H. Sulfur Dioxide Adsorption and Photooxidation on Isotopically-Labeled Titanium Dioxide Nanoparticle Surfaces: Roles of Surface Hydroxyl Groups and Adsorbed Water in the Formation and Stability of Adsorbed Sulfite and Sulfate. *Phys. Chem. Chem. Phys.* **2012**, *14*, 6957−6966.

(13) Prather, K. A.; Hatch, C. D.; Grassian, V. H. Analysis of Atmospheric Aerosols. *Annu. Rev. Anal. Chem.* **2008**, *1*, 485−514.

(14) Formenti, P.; Schutz, L.; Balkanski, Y.; Desboeufs, K.; Ebert, M.; Kandler, K.; Petzold, A.; Scheuvens, D.; Weinbruch, S.; Zhang, D. Recent Progress in Understanding Physical and Chemical Properties of African and Asian Mineral Dust. *Atmos. Chem. Phys.* **2011**, *11*, 8231−8256.

(15) Lee, S.-H.; Murphy, D. M.; Thomson, D. S.; Middlebrook, A. M. Chemical Components of Single Particles Measured with Particle Analysis by Laser Mass Spectrometry (Palms) During the Atlanta Supersite Project: Focus on Organic/Sulfate, Lead, Soot, and Mineral Particles. *J. Geophys. Res.: Atmos.* **2002**, *107*, AAC 1−1−AAC 1−13.

(16) Russell, L. M.; Maria, S. F.; Myneni, S. C. B. Mapping Organic Coatings on Atmospheric Particles. *Geophys. Res. Lett.* **2002**, *29*, 26−21−26−24.

(17) Kubicki, J. D.; Blake, G. A.; Apitz, S. E. Molecular Orbital Calculations for Modeling Acetate−Aluminosilicate Adsorption and Dissolution Reactions. *Geochim. Cosmochim. Acta* **1997**, *61*, 1031−1046.

(18) Chebbi, A.; Carlier, P. Carboxylic Acids in the Troposphere, Occurrence, Sources, and Sinks: A Review. *Atmos. Environ.* **1996**, *30*, 4233−4249.

(19) Nolte, C. G.; Solomon, P. A.; Fall, T.; Salmon, L. G.; Cass, G. R. Seasonal and Spatial Characteristics of Formic and Acetic Acids Concentrations in the Southern California Atmosphere. *Environ. Sci. Technol.* **1997**, *31*, 2547−2553.

(20) Tuazon, E. C.; Winer, A. M.; Pitts, J. N. Trace Pollutant Concentrations in a Multiday Smog Episode in the California South Coast Air Basin by Long Path-Length Fourier-Transform Infrared-Spectroscopy. *Environ. Sci. Technol.* **1981**, *15*, 1232−1237.

(21) Usher, C. R.; Baltrusaitis, J.; Grassian, V. H. Spatially Resolved Product Formation in the Reaction of Formic Acid with Calcium Carbonate ($10\bar{1}4$): The Role of Step Density and Adsorbed Water-Assisted Ion Mobility. *Langmuir* **2007**, *23*, 7039−7045.

(22) Keene, W. C.; Galloway, J. N.; Holden, J. D. Measurement of Weak Organic Acidity in Precipitation from Remote Areas of the World. *J. Geophys. Res.* **1983**, *88*, 5122−5130.

(23) Keene, W. C.; Galloway, J. N. Organic Acidity in Precipitation of North-America. *Atmos. Environ.* **1984**, *18*, 2491−2497.

(24) Kley, D. Tropospheric Chemistry and Transport. *Science* **1997**, *276*, 1043−1045.
(25) FinlaysonPitts, B. J.; Pitts, J. N. Tropospheric Air Pollution: Ozone, Airborne Toxics, Polycyclic Aromatic Hydrocarbons, and Particles. *Science* **1997**, *276*, 1045−1052.
(26) Wu, L.-Y.; Tong, S.-R.; Hou, S.-Q.; Ge, M.-F. Influence of Temperature on the Heterogeneous Reaction of Formic Acid on $\alpha$-$Al_2O_3$. *J. Phys. Chem. A* **2012**, *116*, 10390−10396.
(27) Grosjean, D. Formic-Acid and Acetic-Acid: Emissions, Atmospheric Formation and Dry Deposition at 2 Southern California Locations. *Atmos. Environ.* **1992**, *26*, 3279−3286.
(28) Jacob, D. J.; Wofsy, S. C. Photochemistry of Biogenic Emissions over the Amazon Forest. *J. Geophys. Res.* **1988**, *93*, 1477−1486.
(29) Jacob, D. J. Chemistry of OH in Remote Clouds and Its Role in the Production of Formic-Acid and Peroxymonosulfate. *J. Geophys. Res.* **1986**, *91*, 9807−9826.
(30) Al-Hosney, H. A.; Carlos-Cuellar, S.; Baltrusaitis, J.; Grassian, V. H. Heterogeneous Uptake and Reactivity of Formic Acid on Calcium Carbonate Particles: A Knudsen Cell Reactor, FTIR and SEM Study. *Phys. Chem. Chem. Phys.* **2005**, *7*, 3587−3595.
(31) Tong, S. R.; Wu, L. Y.; Ge, M. F.; Wang, W. G.; Pu, Z. F. Heterogeneous Chemistry of Monocarboxylic Acids on Alpha-$Al_2O_3$ at Different Relative Humidities. *Atmos. Chem. Phys.* **2010**, *10*, 7561−7574.
(32) Rubasinghege, G.; Grassian, V. H. Role(s) of Adsorbed Water in the Surface Chemistry of Environmental Interfaces. *Chem. Commun.* **2013**, *49*, 3071−3094.
(33) Laskin, A.; Moffet, R. C.; Gilles, M. K.; Fast, J. D.; Zaveri, R. A.; Wang, B. B.; Nigge, P.; Shutthanandan, J. Tropospheric Chemistry of Internally Mixed Sea Salt and Organic Particles: Surprising Reactivity of NaCl with Weak Organic Acids. *J. Geophys. Res.: Atmos.* **2012**, *117*, D15302.
(34) Ma, Q. X.; Liu, Y. C.; Liu, C.; He, H. Heterogeneous Reaction of Acetic Acid on MgO, alpha-$Al_2O_3$, and $CaCO_3$ and the Effect on the Hygroscopic Behaviour of These Particles. *Phys. Chem. Chem. Phys.* **2012**, *14*, 8403−8409.
(35) Wijenayaka, L. A.; Rubasinghege, G.; Baltrusaitis, J.; Grassian, V. H. Surface Chemistry of $\alpha$-Feooh Nanorods and Microrods with Gas-Phase Nitric Acid and Water Vapor: Insights into the Role of Particle Size, Surface Structure, and Surface Hydroxyl Groups in the Adsorption and Reactivity of $\alpha$-FeOOH with Atmospheric Gases. *J. Phys. Chem. C* **2012**, *116*, 12566−12577.
(36) Schuttlefield, J.; Al-Hosney, H.; Zachariah, A.; Grassian, V. H. Attenuated Total Reflection Fourier Transform Infrared Spectroscopy to Investigate Water Uptake and Phase Transitions in Atmospherically Relevant Particles. *Appl. Spectrosc.* **2007**, *61*, 283−292.
(37) Navea, J. G.; Chen, H.; Huang, M.; Carmichel, G. R.; Grassian, V. H. A Comparative Evaluation of Water Uptake on Several Mineral Dust Sources. *Environ. Chem.* **2010**, *7*, 162−170.
(38) Dovesi, R.; Saunders, V. R.; Roetti, R.; Orlando, R.; Zicovich-Wilson, C. M.; Pascale, F.; Civalleri, B.; Doll, K.; Harrison, N. M.; Bush, I. J. *Crystal09 Users Manual*; University of Torino, Torino, Italy, 2009.
(39) Dovesi, R.; Orlando, R.; Civalleri, B.; Roetti, C.; Saunders, V. R.; Zicovich-Wilson, C. M. Crystal: A Computational Tool for the ab Initio Study of the Electronic Properties of Crystals. *Kristallogr.* **2005**, *220*, 571−573.
(40) Catti, M.; Valerio, G.; Dovesi, R.; Causa, M. Quantum-Mechanical Calculation of the Solid-State Equilibrium MgO + alpha-$Al_2O_3 \rightleftharpoons MgAl_2O_4$ (Spinel) Versus Pressure. *Phys. Rev. B: Condens. Matter* **1994**, *49*, 14179−14187.
(41) Gatti, C.; Saunders, V. R.; Roetti, C. Crystal Field Effects on the Topological Properties of the Electron Density in Molecular Crystals: The Case of Urea. *J. Chem. Phys.* **1994**, *101*, 10686−10696.
(42) Lee, C.; Yang, W.; Parr, R. G. Development of the Colle−Salvetti Correlation-Energy Formula into a Functional of the Electron Density. *Phys. Rev. B* **1988**, *37*, 785−789.
(43) Becke, A. D. Density-Functional Thermochemistry. III. The Role of Exact Exchange. *J. Chem. Phys.* **1993**, *98*, 5648−5652.
(44) Monkhorst, H. J.; Pack, J. D. Special Points for Brillouin-Zone Integrations. *Phys. Rev. B* **1976**, *13*, 5188.
(45) Civalleri, B.; D'Arco, P.; Orlando, R.; Saunders, V. R.; Dovesi, R. Hartree-Fock Geometry Optimisation of Periodic Systems with the Crystal Code. *Chem. Phys. Lett.* **2001**, *348*, 131−138.
(46) Doll, K.; Saunders, V. R.; Harrison, N. M. Analytical Hartree−Fock Gradients for Periodic Systems. *Int. J. Quantum Chem.* **2001**, *82*, 1−13.
(47) Doll, K. Implementation of Analytical Hartree-Fock Gradients for Periodic Systems. *Comput. Phys. Commun.* **2001**, *137*, 74−88.
(48) Broyden, C. G. The Convergence of a Class of Double-Rank Minimization Algorithms 1. General Considerations. *IMA J. Appl. Math.* **1970**, *6*, 76−90.
(49) Fletcher, R. A New Approach to Variable Metric Algorithms. *Comput. J.* **1970**, *13*, 317−322.
(50) Goldfarb, D. A Family of Variable-Metric Methods Derived by Variational Means. *Math. Comput.* **1970**, *24*, 23−26.
(51) Shanno, D. F. Conditioning of Quasi-Newton Methods for Function Minimization. *Math. Comput.* **1970**, *24*, 647−656.
(52) Digne, M.; Sautet, P.; Raybaud, P.; Euzen, P.; Toulhoat, H. Use of DFT to Achieve a Rational Understanding of Acid−Basic Properties of Γ-Alumina Surfaces. *J. Catal.* **2004**, *226*, 54−68.
(53) Frisch, M. J.; Trucks, G. W.; Schlegel, H. B.; Scuseria, G. E.; Robb, M. A.; Cheeseman, J. R.; Scalmani, G.; Barone, V.; Mennucci, B.; Petersson, G. A.; Nakatsuji, H.; et al. *Gaussian 09*, revision B.01; Gaussian, Inc: Wallingford, CT, 2010.
(54) Zhao, Y.; Schultz, N. E.; Truhlar, D. G. Design of Density Functionals by Combining the Method of Constraint Satisfaction with Parametrization for Thermochemistry, Thermochemical Kinetics, and Noncovalent Interactions. *J. Chem. Theory Comput.* **2006**, *2*, 364−382.
(55) Hudson, P. K.; Gibson, E. R.; Young, M. A.; Kleiber, P. D.; Grassian, V. H. Coupled Infrared Extinction and Size Distribution Measurements for Several Clay Components of Mineral Dust Aerosol. *J. Geophys. Res.: Atmos.* **2008**, *113*, D01201.
(56) Schuttlefield, J. D.; Cox, D.; Grassian, V. H. An Investigation of Water Uptake on Clays Minerals Using ATR-FTIR Spectroscopy Coupled with Quartz Crystal Microbalance Measurements. *J. Geophys. Res.: Atmos.* **2007**, *112*, D21303.
(57) Frost, R. L.; Kloprogee, J. T. Raman and Spectroscopic Study of the Modification of Kaolinite Surfaces by Intercalation with Organic Molecules. In *Encyclopedia of Surface and Colloid Science*; Hubbard, A. T., Ed.; Marcel Dekker AG: New York, 2002; Vol. *4*, pp 4438−4451.
(58) Schroeder, P. A. Infrared Spectroscopy in Clay Science. In *CMS Workshop Lectures*; Rule, A., Guggenheim, S., Eds.; The Clay Mineral Society: Aurora, CO, 2002; Vol. *11*, pp 181−206.
(59) White, C. E.; Provis, J. L.; Riley, D. P.; Kearley, G. J.; van Deventer, J. S. J. What Is the Structure of Kaolinite? Reconciling Theory and Experiment. *J. Phys. Chem. B* **2009**, *113*, 6756−6765.
(60) Madejova, J.; Komadel, P. Baseline Studies of the Clay Minerals Society Source Clays: Infrared Methods. *Clays Clay Miner.* **2001**, *49*, 410−432.
(61) Iuga, C.; Sainz-Diaz, C. I.; Vivier-Bunge, A. Interaction Energies and Spectroscopic Effects in the Adsorption of Formic Acid on Mineral Aerosol Surface Models. *J. Phys. Chem. C* **2012**, *116*, 2904−2914.
(62) Reva, I. D.; Plokhotnichenko, A. M.; Radchenko, E. D.; Sheina, G. G.; Blagoi, Y. P. The IR Spectrum of Formic Acid in an Argon Matrix. *Spectrochim. Acta, Part A* **1994**, *50*, 1107−1111.
(63) Li, G. X.; Ridd, M. J.; Larkins, F. P. An Infrared Study of Formic-Acid Adsorption on $Co/SiO_2$ and $SiO_2$ Surfaces. *Aust. J. Chem.* **1991**, *44*, 623−626.
(64) Chapman, D. The Infrared Spectra of Liquid and Solid Formic Acid. *J. Chem. Soc.* **1956**, 225−229.
(65) Millikan, R. C.; Pitzer, K. S. The Infrared Spectra of Dimeric and Crystalline Formic Acid. *J. Am. Chem. Soc.* **1958**, *80*, 3515−3521.
(66) Amenomiya, Y. Active-Sites of Solid Acidic Catalysts 0.3. Infrared Study of the Water Gas Conversion Reaction on Alumina. *J. Catal.* **1979**, *57*, 64−71.

(67) Chauvin, C.; Saussey, J.; Lavalley, J. C.; Idriss, H.; Hindermann, J. P.; Kiennemann, A.; Chaumette, P.; Courty, P. Combined Infrared-Spectroscopy, Chemical Trapping, and Thermoprogrammed Desorption Studies of Methanol Adsorption and Decomposition on $ZnAl_2O_4$ and $Cu/ZnAl_2O_4$ Catalysts. *J. Catal.* **1990**, *121*, 56−69.
(68) Walmsley, D. G.; Nelson, W. J.; Brown, N. M. D.; Decheveigne, S.; Gauthier, S.; Klein, J.; Leger, A. Evidence from Inelastic Electron Tunnelling Spectroscopy for Vibrational-Mode Reassignments in Simple Aliphatic Carboxylate Ions. *Spectrochim. Acta, Part A* **1981**, *37*, 1015−1019.
(69) Klein, J.; Leger, A.; Belin, M.; Defourne., D.; Sangster, M. J. Inelastic-Electron-Tunneling Spectroscopy of Metal-Insulator-Metal Junctions. *Phys. Rev. B* **1973**, *7*, 2336−2348.
(70) Gao, H.; Yan, T.; Yu, Y.; He, H. DFT and DRIFTS Studies on the Adsorption of Acetate on the $Ag/Al_2O_3$ Catalyst. *J. Phys. Chem. C* **2008**, *112*, 6933−6938.
(71) Hedberg, J.; Baldelli, S.; Leygraf, C. Initial Atmospheric Corrosion of Zn: Influence of Humidity on the Adsorption of Formic Acid Studied by Vibrational Sum Frequency Spectroscopy. *J. Phys. Chem. C* **2009**, *113*, 6169−6173.
(72) Baltrusaitis, J.; Schuttlefield, J.; Jensen, J. H.; Grassian, V. H. Ftir Spectroscopy Combined with Quantum Chemical Calculations to Investigate Adsorbed Nitrate on Aluminium Oxide Surfaces in the Presence and Absence of Co-Adsorbed Water. *Phys. Chem. Chem. Phys.* **2007**, *9*, 4970−4980.
(73) Shimanouchi, T. Molecular Vibrational Frequencies. *NIST Chemistry Webbook*, NIST Standard Reference Database Number 69; Linstrom, P. J., Mallard, W. G., Eds.; National Institute of Standards and Technology: Gaithersburg, MD, 20899.
(74) Baltrusaitis, J.; Jensen, J. H.; Grassian, V. H. Ftir Spectroscopy Combined with Isotope Labeling and Quantum Chemical Calculations to Investigate Adsorbed Bicarbonate Formation Following Reaction of Carbon Dioxide with Surface Hydroxyl Groups on $Fe_2O_3$ and $Al_2O_3$. *J. Phys. Chem. B* **2006**, *110*, 12005−12016.
(75) Wong, M. W. Vibrational Frequency Prediction Using Density Functional Theory. *Chem. Phys. Lett.* **1996**, *256*, 391−399.
(76) Alecu, I. M.; Zheng, J.; Zhao, Y.; Truhlar, D. G. Computational Thermochemistry: Scale Factor Databases and Scale Factors for Vibrational Frequencies Obtained from Electronic Model Chemistries. *J. Chem. Theory Comput.* **2010**, *6*, 2872−2887.
(77) *Theory, Operation and Calibration in QCM200 Quartz Crystal Microbalance Digital Controller Operation and Service Manual*; Stanford Research Systems: Sunnyvale, CA, 2005; pp 15−49.
(78) Borensen, C.; Kirchner, U.; Scheer, V.; Vogt, R.; Zellner, R. Mechanism and Kinetics of the Reactions of $NO_2$ or $HNO_3$ with Alumina as a Mineral Dust Model Compound. *J. Phys. Chem. A* **2000**, *104*, 5036−5045.
(79) Morterra, C.; Magnacca, G. A Case Study: Surface Chemistry and Surface Structure of Catalytic Aluminas, as Studied by Vibrational Spectroscopy of Adsorbed Species. *Catal. Today* **1996**, *27*, 497−532.
(80) Knozinger, H.; Ratnasamy, P. Catalytic Aluminas: Surface Models and Characterization of Surface Sites. *Catal. Rev.* **1978**, *17*, 31−70.
(81) Datka, J.; Sarbak, Z.; Eischens, R. P. Infrared Study of Coke on Alumina and Zeolite. *J. Catal.* **1994**, *145*, 544−550.
(82) Laskin, A.; Iedema, M. J.; Ichkovich, A.; Graber, E. R.; Taraniuk, I.; Rudich, Y. Direct Observation of Completely Processed Calcium Carbonate Dust Particles. *Faraday Discuss.* **2005**, *130*, 453−468.
(83) Li, W. J.; Shao, L. Y. Observation of Nitrate Coatings on Atmospheric Mineral Dust Particles. *Atmos. Chem. Phys.* **2009**, *9*, 1863−1871.
(84) Li, W.; Shao, L. Mixing and Water-Soluble Characteristics of Particulate Organic Compounds in Individual Urban Aerosol Particles. *J. Geophys. Res.* **2010**, *115*.